Journal of Magnetism and Magnetic Materials 603 (2024) 172203

Contents lists available at ScienceDirect

Journal of Magnetism and Magnetic Materials

journal homepage: www.elsevier.com/locate/jmmm

Research article

Valence instability and collapse of ferromagnetism in EuB_6 at high pressures

L.O. Kutelak [a,b], R. Sereika [c], G. Fabbris [d], L. Francisco [a,b], G. Lombardi [a,b], E.H.T. Poldi [a,b], J. Zhao [d], E.E. Alp [d], N.M. Souza Neto [a], P.F.S. Rosa [e], D. Haskel [d], W. Bi [c], R.D. dos Reis [a,*]

[a] Brazilian Synchrotron Light Laboratory (LNLS), Brazilian Center for Research in Energy and Materials (CNPEM), Campinas, Sao Paulo, Brazil
[b] Instituto de Fisica Gleb Wataghin, Universidade Estadual de Campinas (UNICAMP), SP, Brazil
[c] Department of Physics, University of Alabama at Birmingham, Birmingham, AL 35294, USA
[d] Advanced Photon Source, Argonne National Laboratory, Argonne, IL, 60439, USA
[e] Los Alamos National Laboratory - Los Alamos, NM 87545, USA

ARTICLE INFO

Keywords:
Valence instabilities
Magnetic transitions
Ferromagnetism collapse
High pressure spectroscopy

ABSTRACT

Despite the simplicity of their cubic crystal lattice, rare-earth hexaborides display complex physical properties including a (long debated) onset of metallization via magnetic polaron formation at $T_{c1} \approx 15$ K preceding ferromagnetic ordering at $T_{c2} \approx 12$ K. In this work, we used applied pressure to tune the interplay between electronic structure and magnetism in EuB_6. We probed the magnetism, valence, and structure of EuB_6 under quasi-hydrostatic pressures up to 30 GPa using X-ray techniques. Our findings show evidence for collapse of ferromagnetism above 20 GPa following a monotonic increase of mean Eu valence. While X-ray diffraction measurements in the paramagnetic state at room temperature show that the lattice retains cubic symmetry, a measurable quadrupole interaction seen by time-domain synchrotron Mössbauer spectroscopy suggests a lowering of symmetry associated with magnetic ordering, becoming more prominent across the magnetic transition. The interplay between conduction band electron count and magnetism observed under applied pressure in EuB_6 opens possibilities for fine-tuning metallization and magnetic properties of similar Eu-based semi-metal systems.

1. Introduction

EuB_6 is the representative ferromagnetic member within the family of rare-earth hexaborides, which exhibits a plethora of puzzling transport, magnetic and topological properties such as the proposed topological Kondo insulator behavior [1–15]. EuB_6 has a long history of experimental puzzles, such as the two-step transition at $T_{c1} = 15.3$ K and $T_{c2} = 12.5$ K. Initially, it was believed that T_{c1} originated from magnetic ordering, while T_{c2} occurred due to a reorientation of the magnetization direction [16]. Later, it was argued that the higher temperature transition is attributed to the material's metallization through the overlap of magnetic polarons, resulting in $T_{c2} = 12.5$ K as the actual magnetic ordering temperature [17], which is in agreement with T_c obtained by neutron diffraction [18]. Further evidence for magnetic polarons has been reported by scanning tunneling microscopy [19], magneto optical imaging [20], Raman scattering [21], and magnetoresistance [22]. Experiments with Yb doping further supports the separation between magnetic ordering and metallization [23] suggesting polaron overlap and subsequent magnetic ordering is the most likely scenario.

Recently it was suggested that non-trivial topological phases may arise in special conditions of magnetization direction as long as specific mirror symmetries are conserved [24–26]. A change in magnetization direction may turn EuB_6 from a topological nodal-line semiconductor to a Weyl semimetal [24]. Compressing the lattice while conserving crystal structure using hydrostatic pressure is a convenient route to tune magnetic and electronic properties which might generate changes in topology.

High pressure electrical resistivity experiments showed an increase of both transition temperatures up to pressures of about 5 GPa. At higher pressures up to 17 GPa, both transition temperatures remain unchanged [27]. It is suggested that the Ruderman–Kittel–Kasuya–Yosida (RKKY) interaction is responsible for the magnetism of the sample, with electronic density at the X point of the Brillouin zone, which hosts electron and hole pockets [28,29], playing a main role for the changes in the interaction. Notably, carbon doping turns EuB_6 into an antiferromagnet [30] and band structure calculations of pure EuB_6 reveal the presence of two effective exchange couplings between 4*f* moments and itinerant electrons: a parallel (ferromagnetic) coupling to

* Corresponding author.
E-mail address: ricardo.reis@lnls.br (R.D. dos Reis).

https://doi.org/10.1016/j.jmmm.2024.172203
Received 30 March 2024; Received in revised form 21 May 2024; Accepted 28 May 2024
Available online 5 June 2024
0304-8853/© 2024 Elsevier B.V. All rights are reserved, including those for text and data mining, AI training, and similar technologies.

conduction electrons and an antiparallel (antiferromagnetic) coupling to valence electrons [31].

Applied hydrostatic pressure is a clean, symmetry-preserving tuning parameter that not only provides information about the evolution of magnetic phases but also holds the promise to unveil new emergent phenomena. The simple cubic structure ($Pm\bar{3}m$) seems ideal for hydrostatic pressure experiments with evidence for structural sturdiness in CeB_6, which shares the same structure and shows no structural transitions up to at least 85 GPa of applied pressure [32]. In this work, quasi-hydrostatic pressures to 30 GPa were applied to high-quality Al-flux grown samples of EuB_6 [33,34], in which single crystals were mechanically crushed into powdered form. We utilized a range of synchrotron techniques including X-ray absorption near edge spectroscopy (XANES), X-ray magnetic circular dichroism (XMCD), X-ray diffraction (XRD) and time-domain synchrotron Mössbauer spectroscopy (SMS), to shed light into the electronic ground state of EuB_6 under high pressures and low temperatures. The experimental data gathered provide insights into the evolution of electronic and magnetic properties such as an observed increase in mean valence above 10 GPa and collapse of ferromagnetic ordering at 20 GPa, with likely emergence of antiferromagnetic order at higher pressures. Additionally, the observation of a non-zero quadrupole interaction in the SMS data at low temperatures is indicative of lowering of point symmetry at Eu sites which becomes more pronounced above the magnetic transition.

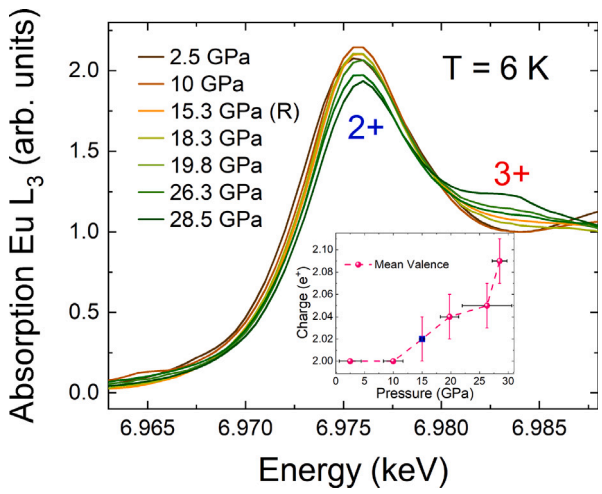

Fig. 1. Eu-L_3 XANES spectra for selected pressure points at 6 K. We observe only one peak at the Eu L_3 edge up to 10.3 GPa associated with a pure 2+ valence state. At higher pressures, a kink around 8 eV above the main peak appears and grows with pressure. Inset shows the valence evolution as a function of pressure obtained by adjusting simulated spectra with experimental data. Simulated data is available in the Supplemental Material [41]. Data point at 15.3 GPa was taken after releasing the pressure from 28.5 GPa.

2. Methods

Single-crystal samples were grown from Al flux as described in Ref. [35,36]. For the different experiments, samples were always selected from the same batch. XANES and XMCD measurements were performed at the 4ID-D beamline [37] of the Advanced Photon Source (APS), Argonne National Laboratory. EuB_6 single crystals were crushed into fine powder and placed inside a miniature diamond anvil cell (DAC) within a laser drilled [38] rhenium gasket for sample support together with silicone oil as pressure transmitting medium. A helium-flow cryostat was used for controlling the sample temperature down to 6 K. Each pressure point was obtained by removing the sample from the cryostat and applying torque at room temperature to the DAC screws. Pressure was measured at room temperature before and after each data collection cycle with the Ruby fluorescence technique [39]. For XMCD experiments, a quarter wave plate was used to generate circularly polarized X-rays of alternating helicity. XMCD data were collected in helicity-switching mode in fixed magnetic field direction. Data were collected in magnetic field up to 4 T applied either along or opposite to the X-ray helicity direction. The redundant reversal of X-ray helicity and magnetic field allows us to rule out artifacts of non-magnetic origin in the XMCD signals. Both XANES and XMCD data were normalized by the difference between post-edge and pre-edge absorption to account for any sample thickness change in the pressure cell at the different applied pressures.

Room temperature X-ray diffraction was performed at the EMA beamline of the Brazilian Synchrotron Light Laboratory, Sirius. A fine powder sample was obtained from single crystals and placed inside a rhenium gasket while utilizing neon gas as pressure medium. A ruby sphere was placed together with sample for pressure measurement and a standard DAC coupled to a gas-membrane system was utilized for pressure application. The X-ray energy was calibrated to a 0.4859 Å wavelength and the beam focused with a KB mirror pair to a 20 × 20 μm^2 focus size at the sample position. The diffraction patterns were then detected with a marCCD mosaic 220. DIOPTAS [40] software was utilized to integrate 2θ intensities from diffraction rings which were limited to an 120 degrees azimuth due to the experiment geometry and CCD placement. More details on the XRD measurements and data analysis are included in the Supplemental Material (SM) [41].

The time-domain synchrotron Mössbauer spectroscopy measurements were performed at the 3ID-B beamline of the APS at the Argonne National Laboratory, using EuB_6 crystals inside a mini-panoramic DAC [42] with helium gas as pressure transmitting media inside the laser-drilled rhenium gasket. The helium flow cryostat base temperature for the SMS measurements was 9 K which is below T_c for EuB_6. The combination of a helium gas membrane and on-line ruby fluorescence detection allowed for in-situ control of pressure at low temperature.

3. Results

The pressure dependence of the Eu valence at T = 6 K was determined using the element and orbital selectivity of X-ray absorption spectroscopy. Results for selected pressure points for the Eu- L_3 absorption edge are shown in Fig. 1. For pressures up to 10 GPa there is only one absorption peak, which is associated with the Eu^{2+} valence. For higher pressures, a shoulder is observed about 8 eV above the L_3 absorption peak (white line), which suggests that the mean valence of Eu is shifting towards a 3+ state in a systematic manner as shown in the inset of Fig. 1. To accurately estimate the Eu valence, we utilized the Finite Difference Method Near Edge Structure (FDMNES) code [43] to perform first principle calculations of the XANES spectra for both Eu valence configurations (2+ and 3+) using the lattice parameters determined by XRD. Then, the theoretical Eu^{2+} and Eu^{3+} XANES spectra were linearly combined to reconstruct the experimental data [44,45]. This method takes into account the different shape of XANES spectra for each of the valence states (further details of this method are included in the SM [41]). Accounting for the different ratio of white line to edge jump for the two valence states it was possible to estimate that the Eu^{3+} contribution at 15 GPa is 2% and reaches 9% at 28.5 GPa. This corresponds to an average valence increase from 2+ at ambient pressure to 2.09+ at 28.5 GPa. This indicates that magnetic Eu^{2+} and non-magnetic Eu^{3+} states coexist in the material. A data point collected after pressure release from 28.5 GPa to 15.3 GPa indicates that the valence change appears to be reversible because the observed satellite peak from Eu^{3+} diminishes in intensity.

Although XANES results strongly suggest that the Eu mean valence increases under applied pressure, a change in structural symmetry and related changes in X-ray absorption fine structure could also cause the appearance of the second absorption peak [46]. To verify the stability of the structure over this pressure range we performed in-situ high pressure synchrotron X-ray powder diffraction up to 30 GPa at ambient

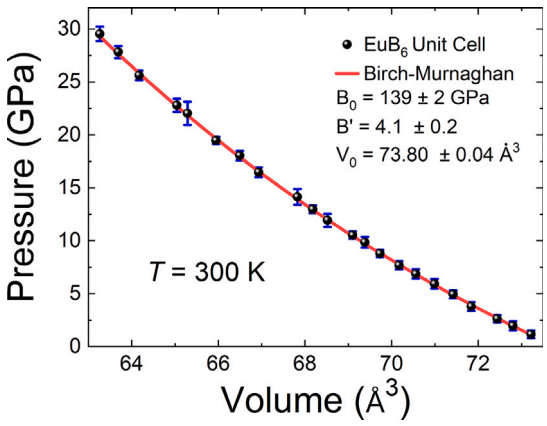

Fig. 2. Applied pressure as a function of unit cell volume for EuB_6. Uncertainties for cell volume are smaller than the points. Red line indicates the fitted curve for a third-order Birch–Murnaghan equation of state.

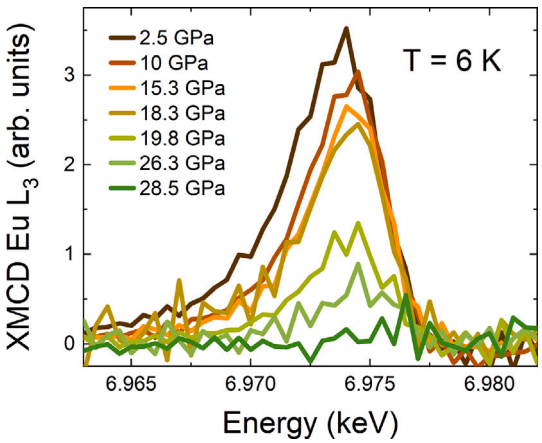

Fig. 3. X-ray magnetic circular dichroism spectra for Eu L_3 absorption edge for selected pressure points at T = 6 K. While a prominent XMCD signal is observed up to 18.3 GPa, the XMCD is suddenly suppressed above that pressure and no XMCD is detected at 28.5 GPa.

temperature. The X-ray difractograms, presented in the SM [41], do not reveal the presence of extra peaks over the entire pressure range studied, indicating that no structural phase transition takes place up to the highest pressure at ambient temperature. It is worth noting that subtle structural changes may take place at low temperature below the magnetic ordering temperature, as pointed out by magnetostriction measurements [22] and Raman measurements [47]. The lack of structural transitions at ambient temperature and the systematic, gradual increase in mean valence over a 20 GPa range, indicate that the changes seen in XANES are associated with a valence evolution and not with a change in atomic arrangement around the Eu absorbing ions. The GSAS-II [48] software was used to perform Le-Bail analysis of our powder diffraction data to obtain the unit cell volume for each of the pressures, which are shown in Fig. 2. It was then possible to fit the derived volumes to a third order Birch–Murnaghan equation of state [32] where the initial volume V_0 was set as a fit parameter because our first pressure point was 1.5 GPa. The best fit of our data provided $B_0 = 139 \pm 2$ GPa, $B_0' = 4.1 \pm 0.2$ and $V_0 = 73.80 \pm 0.04$ Å^3, which is consistent with the recently reported value of $B_0 = 141.0 \pm 0.9$ GPa [49]. These experimental values differ by about 16% from theoretical values of $B_0 = 161$ GPa [31], and $B_0 = 152.4$ GPa and $B_0' = 3.59$ [26].

Because of the valence instability, one might expect changes in the magnetic behavior of the material. Here we used the spin-dependent sensitivity and atomic selectivity of XMCD to probe the magnetic properties of Eu. XMCD spectra probe the empty spin-dependent density of states (DOS) near the Fermi level, as opposed to the spin-averaged empty DOS probed by XANES. Fig. 3 presents the XMCD spectra at the Eu L_3-edge as a function of applied pressure. XMCD data were obtained with an applied magnetic field H = 4 T for all spectra except 2.5 GPa and 10 GPa where H = 1 T was applied. It is worth noting that, as shown by XMCD as function of applied field in Fig. S5 available in the SM [41], magnetization is nearly saturated at 1 T. It is clear that for pressures up to 18.4 GPa there is a dichroic signal. However, at 19.8 GPa a significant drop of XMCD signal is observed and the signal vanishes at 28.5 GPa. The vanishing of XMCD signal indicates loss of net spin polarization in the 5*d* states, namely, vanishing of net magnetization. However, as XMCD only probes the net magnetization, the collapse of XMCD can indicate that the material becomes either antiferromagnetic or paramagnetic. We note that, similarly to what happens for the valence in XANES experiments, when the pressure is released to 10 GPa the XMCD is restored, demonstrating that the transition is reversible.

In order to investigate further the changes in valence and magnetic order time-domain synchrotron Mössbauer Spectroscopy was used to better understand magnetic and electronic characteristics of our sample at high pressures. Mösssbauer spectroscopy relies on the absorption and (delayed) emission of radiation by nuclei of certain isotopes, Eu-151 being one of them. Eu-151 has a 21.54 keV transition between a I = $\frac{7}{2}$ excited state and I = $\frac{5}{2}$ ground state, where I is nuclear spin [50]. Here, we analyze the delayed (half-life τ = 9.7 ns) X-ray emission of Eu nuclei decaying into the ground state. Because nuclear levels split and display hyperfine structure under the influence of magnetic field, and because the emission from transitions between excited and ground split levels is coherent, interference leads to quantum beats in the delayed X-ray emission. Because one can probe Zeeman split nuclear levels, it is possible to determine whether the sample is under the influence of an internal magnetic field. As shown in Fig. 4 a well-defined interference pattern due to quantum beats coming from magnetically split nuclear Zeeman levels is observed between 5 GPa and 18 GPa. Notably, a dramatic change in quantum beat behavior emerges at higher pressures. At 21 GPa, a major difference in the time domain spectra is observed, where the beating due to magnetic splitting appears to be severely suppressed. This results indicate a change in the hyperfine field, in agreement with XMCD data. We note that this hyperfine field arises from three main contributions: the core electron polarization, the polarization of conduction electrons by Europium's electrons, and the polarization of conduction electrons by neighboring atoms [51]. The strong suppression of the hyperfine field at the magnetic transition may be a result of frustration from competing FM and AFM exchange interactions at the critical pressure, resulting in a magnetically disordered phase. For pressures of 24 GPa and 30 GPa quantum beats reappear in the SMS spectra. The possible origin of these quantum beats is discussed below.

Analysis of the time domain spectra was performed utilizing the CONUSS [52] software. SMS fits are also shown in Fig. 4. For data up to 14.5 GPa the fits describe quantum beats reasonably well for almost the entire range of time delays, with exceptions at higher delayed emission times. This is in agreement with the previously reported ferromagnetic behavior of EuB_6 up to these pressures at 9 K [27] and also with our XMCD measurements.

For data at higher pressures, two main models were tested: Model 1 in which EuB_6 becomes antiferromagnetic for pressures higher than 21 GPa, and Model 2, where EuB_6 would become paramagnetic above 21 GPa, with the internal magnetic field strength severely diminished. The fits for Model 1 are depicted in Fig. 4, fits for Model 2 and simulated energy domain spectra equivalent to the time domain SMS spectra for Model 1 are presented in the SM Fig. S12 and S15 respectively [41]. Our model also provides the hyperfine field and quadrupole interaction (QI) eQV_{zz} (where e is the proton charge, Q the nuclear quadrupole

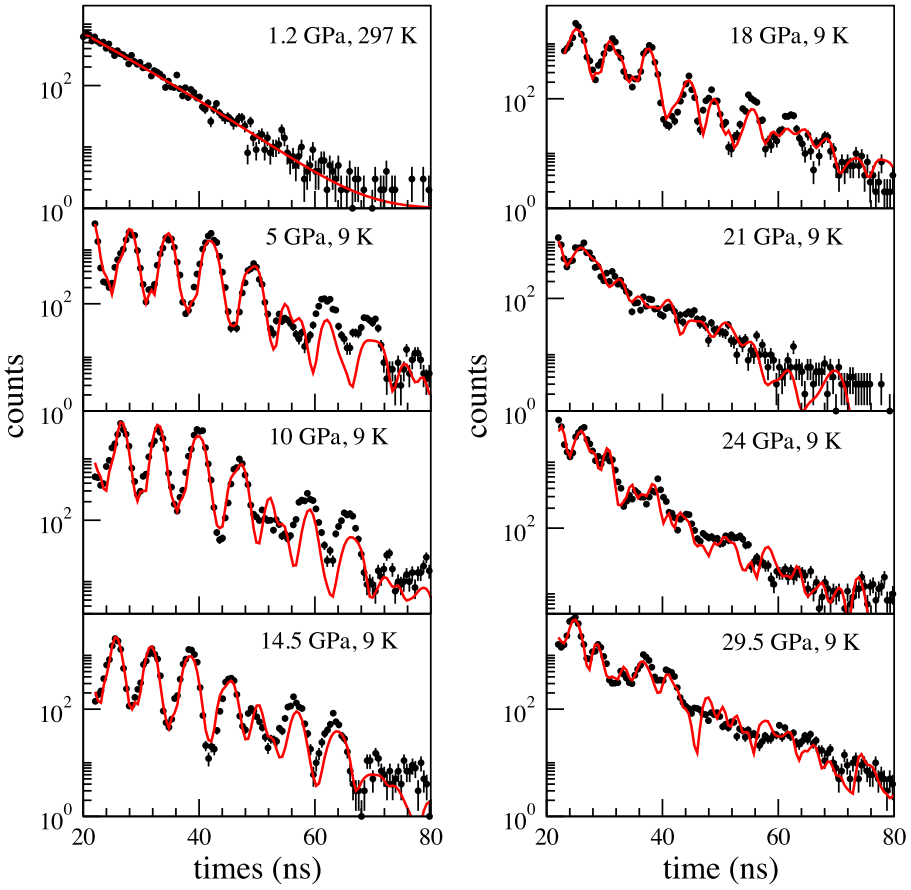

Fig. 4. SMS experimental data (black points) and fits (red lines) using models described in the main text. Fitted hyperfine interaction parameters for the low temperature data are shown in Fig. 5.

moment in the ground state and V_{zz} principal component of the electric field gradient) as function of applied pressure, as shown in Fig. 5. The hyperfine field increases linearly from about 29.1 T at 5 GPa to 33 T at 20 GPa. The low pressure value of the hyperfine field is in reasonable agreement with the reported ambient pressure value of B_{HF} = 26.2 T (T = 4.2 K) in an EuB_6 single crystal [53]. There is then a decrease in hyperfine field in the 18–21 GPa range, of about 30%, followed by a slight increase to 25.6 T at 29.5 GPa. The sudden change in hyperfine field appears to correlate with the disappearance of ferromagnetic order seen in the XMCD data. The QI follows a different trend, starting with a value of 2.7 mm/s at 5 GPa and exhibiting an increase up to 21 GPa. The change in QI appears to correlate more closely with the change in mean valence. It is worth noting that above 21 GPa, the experimental data shows suppressed features and faint beats. From the analysis, we argue that EuB_6 may undergo a magnetic transition from ferromagnetic to antiferromagnetic ordering with lattice contraction, as expected for a metal with RKKY interactions where the exchange coupling between Eu ions depends on interatomic distance and Fermi surface dimensions. Although Model 2 also presents reasonable agreement with experimental data, it would require a rather unphysical strong QI ranging from 43 mm/s up to 45 mm/s. Such a giant QI was reported previously in some Eu compounds such as $EuRh_3B_2$ [54,55], but it is unlikely to occur in EuB_6 because it has a room temperature cubic structure in the $Pm\bar{3}m$ space group with Eu $\bar{3}m$ point symmetry which is unlikely to generate strongly non-spherical distribution for the electric charge around the Eu nuclei. We also note that the Eu-Eu spacing in EuB_6 is much larger (approximately 4 Å) compared to $EuRh_3B_2$ (2 Å). More details about Model 2 are provided in the SM [41]. As mentioned earlier, subtle structural distortions and lowering of Eu point symmetry associated with magnetic ordering are likely to occur in EuB_6 at low temperatures, giving rise to finite QI values also in Model 1. SMS at 1.2 GPa and 297 K in the high temperature, paramagnetic phase (Fig. 4) shows a linear decay without quantum beats indicating negligible QI as a result of cubic point symmetry.

4. Discussion

The combination of XAS and XRD enables the assignment of the changes in XAS under pressure to changes in Eu valence. Specifically, EuB_6 enters a phase where Eu^{2+} and Eu^{3+} coexist above about 10 GPa. The time scale of the XAS measurement is dictated by the $2p_{3/2}$ core-hole lifetime, of about 10^{-16} s. The typical time scale of fluctuating valence between $4f^7$ and $4f^6$ states is about 10^{-11} s [44,56]. XAS time scale being faster than valence fluctuation rates, it cannot distinguish between a static distribution of inequivalent 2+ and 3+ Eu sites, and a single Eu site with fluctuating valence (XAS measures the two components separately as they are separate in absorption energy). Since Eu^{3+} ions are much smaller than Eu^{2+} ions, the scenario with two inequivalent sites would typically require a crystal structure modification or lattice anomalies. In our XRD data, no structural transition or lattice anomaly is observed which makes this possibility highly unlikely. On the other hand, in most divalent Eu compounds, pressure drives Eu to a spatially homogeneous, fluctuating valence state [44,57,58]. We note that the time scale of Mössbauer spectroscopy, dictated by the half-life of the Eu-151 excited nuclear state of 10^{-8} s, is much slower than fluctuating valence rates. Therefore Mössbauer spectroscopy sees a weighted average Eu valence, while XANES will see the individual fluctuating components with their respective weights [59]. Therefore,

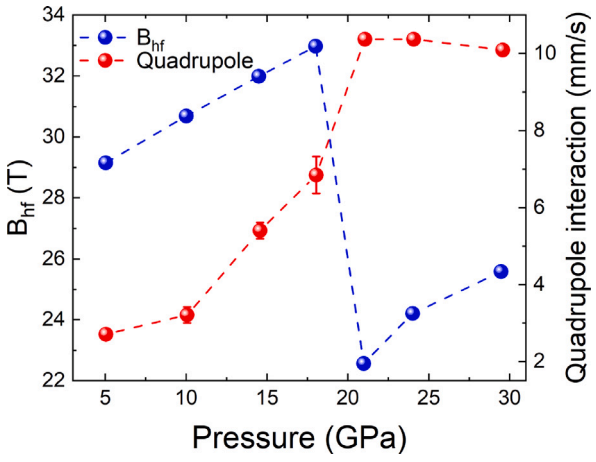

Fig. 5. Pressure evolution of magnetic hyperfine field (left axis) and quadrupole interaction (right axis) as obtained with SMS spectra fitting. It is possible to see a clear change in behavior for both parameters at the 18 GPa mark where B_{hf} decreases while QI sharply increases. Uncertainties for pressures are smaller than the symbols.

in the analysis of time-domain SMS data, only one Eu site was used. We note that, unlike conventional Mössbauer spectroscopy, the isomer shift is not accessible in time-domain SMS experiments unless a reference sample with known valence is measured concomitantly with the EuB_6 sample, which was not done here.

To elucidate the behavior of the electron occupancy in EuB_6 we performed ab-initio DFT simulations utilizing WIEN2k package [60] following the same procedure described in ref [61]. Applied pressure was simulated by decreasing the lattice parameter following the Birch–Murnaghan equation of state, Fig. 2. Our simulations indicate that Eu 5*d* orbital occupation steadily increases while Eu 4*f* decreases as pressure is applied as shown in Table 1. While the trend is consistent with experiment, the change in 4*f* occupation is an order of magnitude smaller than the charge/valence increase seen in XANES. This difference may occur because in our DFT model the 4*f* electrons are treated as well localized core electrons, hence 4*f*-5*d* hybridization is likely to be underestimated. This charge transfer from innermost Eu 4*f* shell and B atoms to 5*d* states and interstitial space is in agreement with previous EuB_6 high pressure studies [27]. More details from our DFT analysis can be found in the SM [41].

Regarding the magnetic ordering, both XMCD and SMS results undoubtedly show that EuB_6 remains a ferromagnet up to 18 GPa, while for higher pressures there is a collapse of the ferromagnetic ordering. Our modeling of the SMS data indicates that the high pressure phase above 20 GPa hosts antiferromagnetic (AFM) ordering. Our modeling indicates that a finite QI is present at low temperature in the magnetically ordered phases, despite cubic symmetry being present at ambient temperature, likely a result of subtle lowering of lattice symmetry driven by magnetic ordering, supported by results from magnetostriction measurements [22]. Another possible source of electric field gradient is a region of valence instability coming from delocalization of charges of Eu and B atoms as suggested by RIXS measurements [62]. While our modeling cannot unambiguously rule out the presence of a paramagnetic phase above 20 GPa, the requirement for a very large, unphysical QI of about 43–45 mm/s makes this scenario highly unlikely.

Additional evidence in support of an AFM high pressure phase comes from XMCD measurements at ambient pressure collected above the magnetic ordering temperature, i.e., in the PM state. In the PM state the applied field at low temperature induces magnetization. As shown in Fig. S5 of SM [41], the induced magnetization at 4 T and low

Table 1
Pressure dependence of orbital occupancies from DFT calculations.

Charge site	0 GPa (e^-)	30 GPa (e^-)
Eu 5*d*	0.2255	0.3071
Eu 4*f*	6.8327	6.7962
Eu total	60.620	60.699
B total	3.455	3.377
Interstitial	11.652	12.037

temperature in the uncorrelated PM state is a significant fraction of the magnetization of the ordered state, a result of the small anisotropy of the spherically symmetric $4f^7$ Eu^{2+} ions. Were the high pressure phase also be PM, we would expect a sizable induced magnetization at 4 T and low T. However, this is not observed and the magnetic susceptibility remains quite small or negligible in the high pressure phase indicative of a correlated state such as AFM. Another argument in favor of an AFM state comes from the fact that usually Eu systems present much higher valence than 2.1+ in the paramagnetic state, as observed in [63].

In addition, as also observed by Cooley et al. [27], despite a T_c value increase for pressures up to 5 GPa, the Curie temperature of the material remains nearly constant in the 5–20 GPa range. The consistent value of ordering temperature at higher pressures may be a result of an interplay between changes in RKKY interaction and valence. Mixed valency under applied pressure increases mixing of 4f and conduction electrons, leading to an increase of indirect exchange coupling J, raising the magnetic ordering temperature, while a shift to non-magnetic Eu^{3+} (magnetic dilution) may act to decrease J. A similar behavior was also observed in the $Eu_{0.5}Yb_{0.5}Ga_4$ compound [61]. Further SMS measurements (shown in Fig. S13 of SM [41]) performed at $T = 20$ K, show the same internal field of the data at T = 9 K at 29.5 GPa. This results indicate that there are no magnetic phase transitions between 9 K and 20 K, which in turn implies that EuB_6 remains in the same magnetic state in this temperature range.

While our interpretation leads us to conclude that AFM order best describes the high pressure phase, we note that this contrasts with the behavior under pressure of other magnetically ordered Eu containing compounds [64] such as $EuRh_2Si_2$ [65], $EuNi_2Si_2$ [66] and $EuCo_2Ge_2$ [67] which present valence shifting towards 3+ but go from a AFM ambient pressure state to a high pressure paramagnetic phase. Meanwhile, ambient pressure FM $EuRu_2P_2$ becomes paramagnetic at 1.5 GPa but also presents a structural transition [68], which is absent in EuB_6. While a coexistence of AFM and FM phases was previously reported in carbon doping experiments [30], such coexistence is incompatible with negligible XMCD signal in the high pressure phase. In order to provide additional evidence in favor of magnetic order in the high pressure phase, additional experimentation using high pressure resonant inelastic X-ray scattering (RIXS) and transport measurements up to 30 GPa and beyond, are highly desired.

5. Summary

In conclusion, by combining XAS, XRD and SMS experiments at pressures up to 30 GPa we demonstrate that both the magnetic ordering and the valence of the EuB_6 compound can be tuned by external pressure without an observable change in structure at room temperature. Further, by extending the pressure range over previous studies, we show an increase in the valence of Eu above about 10 GPa together with the collapse of ferromagnetism near 20 GPa. Open questions that remain include the nature of magnetic ordering in the high pressure phase, which we postulate to be AFM-type based on modeling of SMS data. Additionally, the need to include a quadrupole interaction in the modeling of SMS data indicates that the point symmetry at Eu lattice sites is lower than cubic at low temperature. Since the room temperature crystal structure is cubic at all pressures, this observation is

likely a result of lowering of symmetry by magnetic order, as previously noted in magnetostriction and Raman experiments [22,47]. That the QI not only remains but strengthens in the high pressure phase is another indication that the high pressure low temperature phase hosts magnetic ordering and point symmetry lower than cubic.

Finally, the mechanical control of magnetism and valence for EuB_6 provides a pathway for exploring the connection between magnetic order and topology in this material since the collapse in magnetic order could lead to suppression of topological states [69]. Signatures of such interdependece may appear in transport and mechanism of exchange interactions both in the rare earth hexaboride family as well as in their related compounds.

CRediT authorship contribution statement

L.O. Kutelak: Writing – review & editing, Writing – original draft, Validation, Investigation, Formal analysis, Data curation, Conceptualization. **R. Sereika:** Writing – review & editing, Writing – original draft, Validation, Formal analysis. **G. Fabbris:** Writing – review & editing, Writing – original draft, Formal analysis. **L. Francisco:** Writing – review & editing, Validation, Formal analysis. **G. Lombardi:** Writing – review & editing, Validation, Formal analysis, Data curation. **E.H.T. Poldi:** Writing – review & editing, Formal analysis, Data curation. **J. Zhao:** Writing – review & editing, Investigation, Formal analysis, Data curation. **E.E. Alp:** Writing – review & editing, Validation, Formal analysis. **N.M. Souza Neto:** Writing – review & editing, Validation, Formal analysis. **P.F.S. Rosa:** Writing – review & editing, Writing – original draft, Validation, Formal analysis, Conceptualization. **D. Haskel:** Writing – review & editing, Writing – original draft, Validation, Conceptualization. **W. Bi:** Writing – review & editing, Writing – original draft, Validation, Investigation, Conceptualization. **R.D. dos Reis:** Writing – review & editing, Writing – original draft, Visualization, Validation, Supervision, Project administration, Funding acquisition, Formal analysis, Data curation, Conceptualization.

Declaration of competing interest

The authors declare the following financial interests/personal relationships which may be considered as potential competing interests: Ricardo Donizeth dos Reis reports financial support was provided by State of Sao Paulo Research Foundation. If there are other authors, they declare that they have no known competing financial interests or personal relationships that could have appeared to influence the work reported in this paper.

Data availability

Data will be made available on request.

Acknowledgments

We acknowledge Flavio Gandra, Michael Nicklas and Cristoph Geibel for fruitful discussions. We thank the financial support from the Brazilian agencies CNPq, CAPES and FAPESP, Brazil (Grants 2018/00823-0, 2018/19015-1, 2021/02314-9 and 2022/05447-2). RDdR and L.O.K acknowledges financial support from the Max Planck Society, Germany under the auspices of the Max Planck Partner Group R. D. dos Reis of the MPI for Chemical Physics of Solids, Dresden, Germany. L.F. acknowledge financial support from FAPESP grant 2018/10585-0. E.H.T.P and G.A.L acknowledge financial support from CNPq studentship grant No. 136119/2018-2 and No. 140632/2018-2 respectively. We are grateful to GSECars for the help with gas loading in SMS experiments. Work at Argonne is supported by the U.S. Department of Energy, Office of Science, Office of Basic Energy Sciences, under Contract No. DE-AC-02- 06CH11357. Work at Los Alamos National Laboratory was performed under the auspices of the U.S. Department of Energy, Office of Basic Energy Sciences, Division of Materials Science and Engineering. This research used facilities of the Brazilian Synchrotron Light Laboratory (LNLS), part of the Brazilian Center for Research in Energy and Materials (CNPEM), a private non-profit organization under the supervision of the Brazilian Ministry for Science, Technology, and Innovations (MCTI). The EMA beamline and LCTE staff are acknowledged for the assistance during the experiments 20210101. W.B. acknowledge support from the support from National Science Foundation (NSF), USA CAREER Award No. DMR-2045760.

Appendix A. Supplementary data

Supplementary material related to this article can be found online at https://doi.org/10.1016/j.jmmm.2024.172203.

References

[1] P. Coleman, et al., Handbook of magnetism and advanced magnetic materials, 2007.
[2] M. Dzero, K. Sun, V. Galitski, P. Coleman, Phys. Rev. Lett. 104 (2010) 106408.
[3] K. Flachbart, S. Gabáni, K. Neumaier, Y. Paderno, V. Pavlík, E. Schuberth, N. Shitsevalova, Physica B 378–380 (2006) 610–611.
[4] N. Xu, C.E. Matt, E. Pomjakushina, X. Shi, R.S. Dhaka, N.C. Plumb, M. Radović, P.K. Biswas, D. Evtushinsky, V. Zabolotnyy, J.H. Dil, K. Conder, J. Mesot, H. Ding, M. Shi, Phys. Rev. B 90 (2014) 085148.
[5] J.D. Denlinger, J.W. Allen, J.-S. Kang, K. Sun, B.-I. Min, D.-J. Kim, Z. Fisk, J. Phys. Soc. Japan (2014).
[6] J. Jiang, S. Li, T. Zhang, Z. Sun, F. Chen, Z. Ye, M. Xu, Q. Ge, S. Tan, X. Niu, M. Xia, B. Xie, Y. Li, X. Chen, H. Wen, D. Feng, Nature Commun. 4 (2013) 3010.
[7] K. Chen, T.-C. Weng, G. Schmerber, V.N. Gurin, J.-P. Kappler, Q. Kong, F. Baudelet, A. Polian, L. Nataf, Phys. Rev. B 97 (2018) 235153.
[8] W.T. Fuhrman, J.C. Leiner, J.W. Freeland, M. van Veenendaal, S.M. Koohpayeh, W.A. Phelan, T.M. McQueen, C. Broholm, Phys. Rev. B 99 (2019) 020401.
[9] Y. Li, Q. Ma, S.X. Huang, C.L. Chien, Sci. Adv. 4 (2018).
[10] Y.S. Eo, A. Rakoski, J. Lucien, D. Mihaliov, Ç. Kurdak, P.F.S. Rosa, Z. Fisk, Proc. Natl. Acad. Sci. 116 (2019) 12638–12641.
[11] S. Gabáni, E. Bauer, S. Berger, K. Flachbart, Y. Paderno, C. Paul, V. Pavlík, N. Shitsevalova, Phys. Rev. B 67 (2003) 172406.
[12] N. Harrison, Phys. Rev. Lett. 121 (2018) 026602.
[13] Y. Zhou, P.F.S. Rosa, J. Guo, S. Cai, R. Yu, S. Jiang, K. Yang, A. Li, Q. Si, Q. Wu, Z. Fisk, L. Sun, Phys. Rev. B 101 (2020) 125116.
[14] T. Takimoto, J. Phys. Soc. Japan 80 (2011) 123710.
[15] P.F. Rosa, Z. Fisk, Bulk and surface properties of SmB6, 2020, arXiv preprint arXiv:2007.09137.
[16] S. Süllow, I. Prasad, M.C. Aronson, J.L. Sarrao, Z. Fisk, D. Hristova, A.H. Lacerda, M.F. Hundley, A. Vigliante, D. Gibbs, Phys. Rev. B 57 (1998) 5860–5869.
[17] S. Süllow, I. Prasad, M.C. Aronson, S. Bogdanovich, J.L. Sarrao, Z. Fisk, Phys. Rev. B 62 (2000) 11626–11632.
[18] W. Henggeler, H.-R. Ott, D. Young, Z. Fisk, Solid State Commun. 108 (1998) 929–932.
[19] M. Pohlit, S. Rößler, Y. Ohno, H. Ohno, S. von Molnár, Z. Fisk, J. Müller, S. Wirth, Phys. Rev. Lett. 120 (2018) 257201.
[20] D.J. Sivananda, A. Kumar, M.A. Ali, S.S. Banerjee, P. Das, J. Müller, Z. Fisk, Phys. Rev. Mater. 2 (2018) 113404.
[21] P. Nyhus, S. Yoon, M. Kauffman, S.L. Cooper, Z. Fisk, J. Sarrao, Phys. Rev. B 56 (1997) 2717–2721.
[22] R.S. Manna, P. Das, M. de Souza, F. Schnelle, M. Lang, J. Müller, S. von Molnár, Z. Fisk, Phys. Rev. Lett. 113 (2014) 067202.
[23] M.A. Anisimov, A.V. Bogach, A.V. Kuznetsov, A.N. Azarevich, N.A. Samarin, S.V. Demishev, N.Y. Shitsevalova, A.V. Dukhnenko, V.B. Filipov, N.E. Sluchanko, V.V. Glushkov, Phys. Solid State 61 (2019) 565–570.
[24] S. Nie, Y. Sun, F.B. Prinz, Z. Wang, H. Weng, Z. Fang, X. Dai, Phys. Rev. Lett. 124 (2020) 076403.
[25] Y. Takahashi, M. Fujimoto, M. Tsuchiko, K.-I. Ohshima, J. Appl. Crystallogr. 34 (2001) 208–209.
[26] J. Duan, T. Zhou, L. Zhang, J.-G. Du, G. Jiang, H.-B. Wang, Chin. Phys. B 24 (2015) 096201.
[27] J.C. Cooley, M.C. Aronson, J.L. Sarrao, Z. Fisk, Phys. Rev. B 56 (1997) 14541–14546.
[28] R.G. Goodrich, N. Harrison, J.J. Vuillemin, A. Teklu, D.W. Hall, Z. Fisk, D. Young, J. Sarrao, Phys. Rev. B 58 (1998) 14896–14902.
[29] J.D. Denlinger, G.-H. Gweon, S.-K. Mo, J.W. Allen, J.L. Sarrao, A.D. Bianchi, Z. Fisk, J. Phys. Soc. Japan 71 (2002) 1–4.
[30] M. Kasaya, J. Tarascon, J. Etourneau, P. Hagenmuller, Mater. Res. Bull. 13 (1978) 751–756.
[31] J. Kuneš, W.E. Pickett, Phys. Rev. B 69 (2004) 165111.

[32] N. Foroozani, J. Lim, G. Fabbris, P. Rosa, Z. Fisk, J. Schilling, Physica B 457 (2015) 12–16.
[33] Z. Fisk, D.C. Johnston, B. Cornut, S. von Molnar, S. Oseroff, R. Calvo, J. Appl. Phys. 50 (1979) 1911–1913.
[34] W.A. Phelan, S.M. Koohpayeh, P. Cottingham, J.A. Tutmaher, J.C. Leiner, M.D. Lumsden, C.M. Lavelle, X.P. Wang, C. Hoffmann, M.A. Siegler, N. Haldolaarachchige, D.P. Young, T.M. McQueen, Sci. Rep. 6 (2016) 20860.
[35] Y.S. Eo, A. Rakoski, J. Lucien, D. Mihaliov, Ç. Kurdak, P.F. Rosa, Z. Fisk, Proc. Natl. Acad. Sci. 116 (26) (2019) 12638–12641.
[36] P.F.S. Rosa, Z. Fisk, Flux methods for growth of intermetallic single crystals, 2018, http://dx.doi.org/10.1515/9783110496789-003.
[37] D. Haskel, Y.C. Tseng, N.M. Souza-Neto, J.C. Lang, S. Sinogeikin, Y. Mudryk, K.A. Gschneidner, V.K. Pecharsky, High Press. Res. 28 (2008) 185–192.
[38] R. Hrubiak, S. Sinogeikin, E. Rod, G. Shen, Rev. Sci. Instrum. 86 (2015) 072202.
[39] G. Shen, Y. Wang, A. Dewaele, C. Wu, D.E. Fratanduono, J. Eggert, S. Klotz, K.F. Dziubek, P. Loubeyre, O.V. Fat'yanov, P.D. Asimow, T. Mashimo, R.M.M. Wentzcovitch, High Press. Res. 40 (2020) 299–314.
[40] C. Prescher, V.B. Prakapenka, High Press. Res. 35 (2015) 223–230.
[41] See Supplemental Material at [url] for extra details and datasets.
[42] J.Y. Zhao, W. Bi, S. Sinogeikin, M.Y. Hu, E.E. Alp, X.C. Wang, C.Q. Jin, J.F. Lin, Rev. Sci. Instrum. 88 (2017) 125109.
[43] O. Bunău, Y. Joly, J. Phys.: Condens. Matter. 21 (2009) 345501.
[44] N.M. Souza-Neto, J. Zhao, E.E. Alp, G. Shen, S.V. Sinogeikin, G. Lapertot, D. Haskel, Phys. Rev. Lett. 109 (2012) 026403.
[45] R. dos Reis, L. Veiga, G. Fabbris, F. Garcia, D. Haskel, F. Gandra, N. Souza-Neto, J. Magn. Magn. Mater. 560 (2022) 169619.
[46] W. Bi, N.M. Souza-Neto, D. Haskel, G. Fabbris, E.E. Alp, J. Zhao, R.G. Hennig, M.M. Abd-Elmeguid, Y. Meng, R.W. McCallum, K. Dennis, J.S. Schilling, Phys. Rev. B 85 (2012) 205134.
[47] H. Martinho, C. Rettori, G.M. Dalpian, J.L. Da Silva, Z. Fisk, S.B. Oseroff, J. Phys. Condens. Matter 21 (45) (2009).
[48] B.H. Toby, R.B.V. Dreele, J. Appl. Crystallogr. 46 (2013) 544–549.
[49] R. Sereika, M.P. Clay, L. Zhu, P.F.S. Rosa, W. Bi, Y.K. Vohra, J. Appl. Phys. 134 (13) (2023).
[50] F. Grandjean, G.J. Long, Mössbauer spectroscopy of europium-containing compounds, 1989, http://dx.doi.org/10.1007/978-1-4899-2289-2_11.
[51] W. Bi, J. Lim, G. Fabbris, J. Zhao, D. Haskel, E.E. Alp, M.Y. Hu, P. Chow, Y. Xiao, W. Xu, J.S. Schilling, Phys. Rev. B 93 (18) (2016) 184424.
[52] W. Sturhahn, Hyperfine Interact. 125 (2000) 149–172.
[53] J.M. Coey, O. Massenet, M. Kasaya, J. Etourneau, J. Phys. Colloques 40 (1979) C2–333–C2–336.
[54] S.A. Shaheen, M. Abd-Elmeguid, H. Micklitz, J.S. Schilling, P. Klavins, R.N. Shelton, Phys. Rev. Lett. 55 (1985) 312–315.
[55] S.K. Malik, G.K. Shenoy, S.M. Heald, J.M. Tranquada, Phys. Rev. Lett. 55 (1985) 316–319.
[56] Z. Nix, J. Zhao, E.E. Alp, Y. Xiao, D. Zhang, G.-H. Cao, Y.K. Vohra, W. Bi, J. Phys.: Condens. Matter. 34 (41) (2022) 415601.
[57] Y. Ōnuki, A. Nakamura, F. Honda, D. Aoki, T. Tekeuchi, M. Nakashima, Y. Amako, H. Harima, K. Matsubayashi, Y. Uwatoko, S. Kayama, T. Kagayama, K. Shimizu, S. Esakki Muthu, D. Braithwaite, B. Salce, H. Shiba, T. Yara, Y. Ashitomi, H. Akamine, K. Tomori, M. Hedo, T. Nakama, Phil. Mag. 97 (36) (2017) 3399–3414.
[58] W. Bi, J. Lim, G. Fabbris, J. Zhao, D. Haskel, E.E. Alp, M.Y. Hu, P. Chow, Y. Xiao, W. Xu, J.S. Schilling, Phys. Rev. B 93 (2016) 184424.
[59] D. Haskel, E.A. Stern, H. Shechter, Phys. Rev. B 57 (1998) 8034–8035.
[60] P. Blaha, K. Schwarz, F. Tran, R. Laskowski, G.K.H. Madsen, L.D. Marks, J. Chem. Phys. 152 (2020) 074101.
[61] G. Loula, R. dos Reis, D. Haskel, F. Garcia, N. Souza-Neto, F. Gandra, Phys. Rev. B 85 (24) (2012) 245128.
[62] D. Sheets, V. Flynn, J. Kim, M. Upton, D. Casa, T. Gog, Z. Fisk, M. Dzero, P.F. Rosa, D.G. Mazzone, et al., J. Phys.: Condens. Matter. 32 (13) (2019) 135601.
[63] M. Peters, K. Kliemt, M. Ocker, B. Wolf, P. Puphal, M. Le Tacon, M. Merz, M. Lang, C. Krellner, Phys. Rev. Mater. 7 (6) (2023) 064405.
[64] Y. Ōnuki, M. Hedo, F. Honda, J. Phys. Soc. Japan 89 (10) (2020) 102001.
[65] A. Mitsuda, S. Hamano, N. Araoka, H. Yayama, H. Wada, J. Phys. Soc. Japan 81 (2012) 023709.
[66] A. Nakamura, T. Nakama, K. Uchima, N. Arakaki, C. Zukeran, S. Komesu, M. Takeda, Y. Takaesu, D. Nakamura, M. Hedo, K. Yagasaki, Y. Uwatoko, J. Phys. Conf. Ser. 400 (2012) 032106.
[67] G. Dionicio, H. Wilhelm, Z. Hossain, C. Geibel, Physica B 378–380 (2006) 724–725.
[68] P. Proschek, J. Prchal, M. Diviš, J. Prokleška, K. Vlášková, J. Valenta, J. Zubáč, J. Kaštil, M. Hedo, T. Nakama, et al., J. Alloys Compd. 864 (2021) 158753.
[69] S. Nie, Y. Sun, F.B. Prinz, Z. Wang, H. Weng, Z. Fang, X. Dai, Phys. Rev. Lett. 124 (7) (2020) 076403.